scientific reports

Check for updates

OPEN

Rainfall isotopic variability in northern Central America driven by regionally-organized deep atmospheric convection and airmass rainout

Giuseppe Lucia[1,6]✉, Davide Zanchettin[2], Amos Winter[3], Osmín J. Vásquez[4], Mario Cu-Xi[5] & Matthew S. Lachniet[1]

Understanding the controls of rainfall isotopic composition ($\delta^{18}O_p$) is essential to interpret isotopic paleoclimate records, yet it remains challenging in areas with complex climate and varied topography, such as northern Central America. Here, we present two years of daily rainfall isotope measurements from Guatemala to evaluate the regional and local climatic controls on $\delta^{18}O_p$ variability. We show that regional-scale convection and upstream rainout drive $\delta^{18}O_p$ variability and integrate multi-annual model-based $\delta^{18}O_p$ data supporting a persistent regional control across multiple timescales, from daily to interannual. Further, we document a consistent link between higher rainfall ^{18}O depletion associated with both more intense regionally-organized convective systems and larger stratiform rain fractions. Moisture source analysis shows a dominant contribution from the Caribbean–Atlantic, and secondarily from the Mesoamerican continent, Gulf of Mexico, and Eastern Pacific. While changes between dominant source regions are associated with distinct $\delta^{18}O_p$ signatures, back-trajectory analysis and a source-based isotope reconstruction demonstrate a larger upstream airmass rainout control on the seasonal variations of $\delta^{18}O_p$. Our results suggest that $\delta^{18}O_p$ in Guatemala rainfall are sensitive to regionally-integrated hydroclimatic processes, and that isotope-based paleoclimate records from northern Central America can provide reconstructions of past changes in regional-scale atmospheric convection and upstream rainfall amount.

Stable isotope values of meteoric waters ($H_2{}^{16}O$, $H_2{}^{18}O$, and $HD^{16}O$) are powerful tracers of hydrologic and meteo-climatic processes at multiple spatial and temporal scales[1,2]. Rainwater isotopic composition, defined as $\delta^{18}O_p$ (and δD_p) relative to the Vienna Standard Mean Ocean Water (VSMOW) scale, reflects the distinct mass-dependent isotopic fractionation during phase change processes and airmass rainout effects (i.e., condensation, evaporation, Rayleigh distillation)[3–5]. Isotopic signatures of ancient rainfall can be preserved in terrestrial archives (i.e., ice cores, tree ring cellulose, leaf waxes, speleothems) and are extensively applied as proxies for paleohydrology and paleoclimate changes[6–9]. However, due to potentially complex climatic effects on rainfall $\delta^{18}O_p$, reliable interpretation of isotope proxy records requires a comprehensive understanding of the regional and local climatic controls on modern $\delta^{18}O_p$ composition[10,11].

In the tropics, $\delta^{18}O_p$ variability has been commonly interpreted via the amount effect, that is the negative empirical correlation between local rainfall amount and $\delta^{18}O_p$ at monthly or longer timescales[4,12], underpinning the interpretation of qualitive (wet/dry) paleoclimate changes in many terrestrial isotopic records[13–16]. However, some studies documented weak negative correlations between local rainfall amount and $\delta^{18}O_p$, suggesting that processes other than the amount effect can contribute to tropical $\delta^{18}O_p$ variability[11]. Such processes include changes in moisture source regions[17,18], cloud microphysical processes such as raindrop re-evaporation[11,19], precipitation type[20–22], atmospheric convective intensity[23–26], upstream regional rainfall[27–29], continental

[1]Department of Geoscience, University of Nevada Las Vegas, Las Vegas, NV, USA. [2]Department of Environmental Sciences, Informatics and Statistics, University Ca' Foscari of Venice, Mestre, Italy. [3]Department of Earth and Environmental Systems, Indiana State University, Terre Haute, IN, USA. [4]Centro Universitario del Norte, Universidad de San Carlos de Guatemala, Cobán, Guatemala. [5]Instituto Nacional de Sismología, Vulcanología, Meteorología e Hidrología, Guatemala City, Guatemala. [6]Present address: Jackson School of Geosciences, University of Texas at Austin, Austin, TX, USA. ✉email: luciag1@unlv.nevada.edu

moisture recycling[30,31], and synoptic weather types[32,33]. A further complication is that the processes influencing $\delta^{18}O_p$ variability are spatially heterogenous, so that site-specific studies are needed to disentangle the often-competing controls on $\delta^{18}O_p$. Therefore, identification of key drivers of regional and local $\delta^{18}O_p$ variability in the tropics remains a topic of debate and ongoing research, and a prerequisite to the dynamical interpretation of $\delta^{18}O$ changes in tropical paleoclimate records such as speleothems, lake sediments, tree rings, etc.

Understanding the controls on $\delta^{18}O_p$ is particularly challenging in regions of physiographic and climatic complexity such as Central America, where isotope data are spatially and temporally sparse and the narrow landmass has high topographic relief and proximity to both the Pacific and Atlantic oceans. Modern isotope records exist in the region, mostly from Panama[34], Costa Rica[35], Mexico[36,37], and El Salvador[37]. Integrated studies of rainfall, surface waters, and groundwater isotope data from Mexico[36,38], Guatemala and Belize[37], and the Central American Isthmus[39–41] exhibit decreases in $\delta^{18}O$ from the Caribbean to the Pacific coast, consistent with the progressive temperature-related Rayleigh distillation of Caribbean-sourced moisture moving inland and at higher elevations of the Continental Divide[37–39,41,42]. Although the amount effect has been described at various Central American locations[37,40], rainfall amount-$\delta^{18}O_p$ correlations broadly diverge between sites, suggesting that other climatic and dynamical processes may exert additional controls on $\delta^{18}O_p$ composition. For instance, long-term seasonal $\delta^{18}O_p$ variations over the Panama Isthmus were attributed to sea-surface temperature anomalies in the Caribbean and Eastern Pacific and to the seasonal migration and intensity of convection in the Intertropical Convergence Zone (ITCZ)[34].

Analysis of daily-to-weekly rainfall isotope values from Costa Rica[43,44] showed that seasonal changes in moisture source regions, moisture transport dynamics, and local climate conditions such as the lifting condensation level and surface relative humidity are key drivers of short-term $\delta^{18}O_p$ variability. Other studies from the Central American Isthmus also highlighted the role of stratiform rain fraction within large-scale convective systems as primary controls of rainfall isotope composition[21,45,46]. However, the extent to which each of these processes control rainfall isotopic variability in northern Central America is still poorly understood.

In this study, we present a two-year isotope record (2021–2023) of daily rainfall from Guatemala (Fig. 1) and examine climatic and dynamical processes influencing $\delta^{18}O_p$ variations. We further integrate our two-year observations with a 26-year (1998–2024) modeled $\delta^{18}O_p$ analysis from IsoGSM4[47] to show that regionally-integrated atmospheric convective strength, defined as the regional deep convection within large-scale or mesoscale convective systems (MCS), and upstream rainfall amount control $\delta^{18}O_p$ variability on multiple timescales, from daily to interannual. Because of this strong causality, we conclude that isotopic paleoclimate records in terrestrial archives such as speleothems, tree rings, and lake sediments from northern Central America should provide robust histories of past changes in regional convection, upstream rainout, and regional precipitation amount.

Results and discussion

Seasonality and regional amount effect on Guatemalan rainfall isotopes

We collected daily rainfall samples at Cobán, Alta Verapaz, Guatemala in a Palmex rainwater collector optimized to prevent evaporation (see Sect. "Methods"). Rainwater isotope values ranged from − 17.8 to + 2.6 ‰ for $\delta^{18}O$ and − 127.3 to + 32.3 ‰ for δD, with average values of − 4.38 ± 3.8‰ (1σ) and − 20.3 ± 30.5 ‰ (1σ), respectively. The data define a Local Meteoric Water Line (LMWL) of $\delta D = 8.23 \times \delta^{18}O + 15.7$ ($R^2 = 0.98$, $p < 0.01$; Fig. 2a) that is consistent with previously published LMWLs based on daily and monthly data from Central America[37,38,42–44].

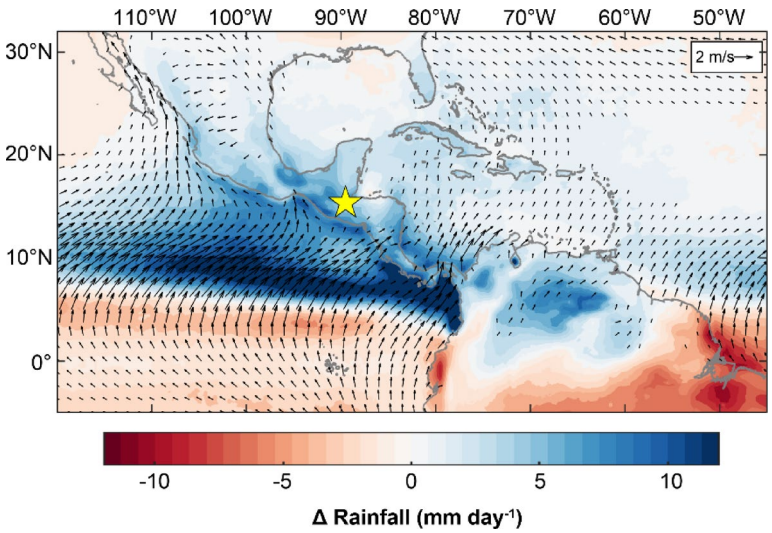


Fig. 1. Climate settings of the study area. Wet (May–November) minus dry (December–April) rainfall and surface wind fields for the climatological period 1998–2024. Yellow star is Cobán (Alta Verapaz, Guatemala). The wet season is associated with higher rainfall and weakened easterly trade winds. Wind vectors below 1 m/s are not displayed for clarity. *Data source*: NASA GPM-IMERG V07.

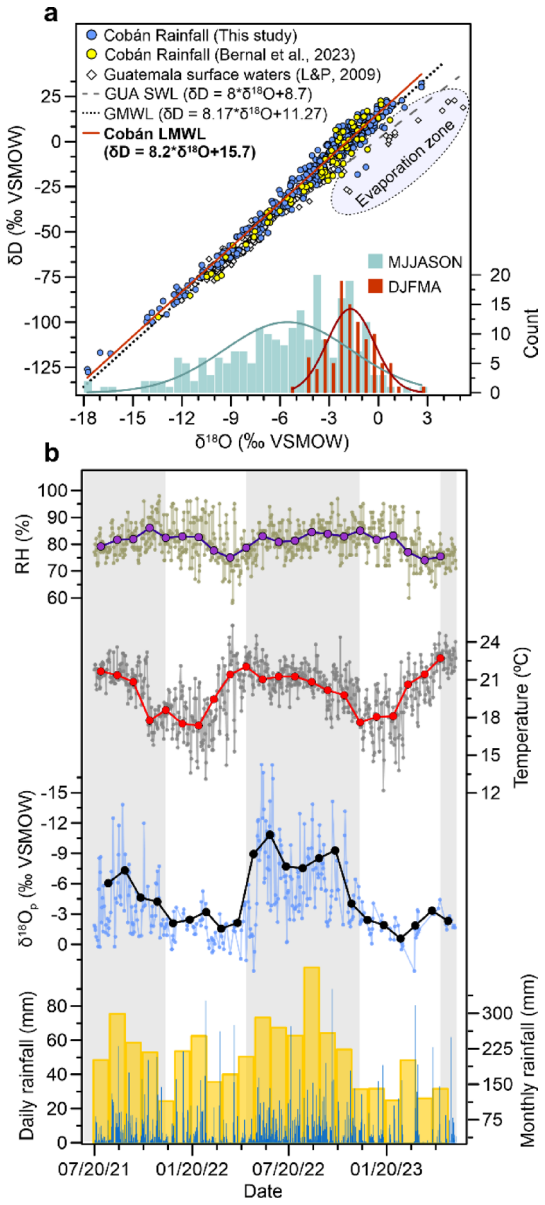


Fig. 2. Guatemalan water isotopes and seasonal hydroclimate at Cobán. (**a**) δ^{18}O-δD relationship in Guatemalan waters: Cobán rainfall for 2021–2023 (blue circles; this study) and 2012 (yellow circles; Bernal et al., 2023), and surface waters (white diamonds; Lachniet and Patterson, 2009). Cobán local meteoric water line (LMWL; solid red) is shown relative to the Global meteoric water line (GMWL; dotted black) and the Guatemala surface water line (GUA SWL; dashed grey). Samples plotting in the evaporation zone indicate potential post-condensation kinetic effects. Overlapping histograms of 2021–2023 seasonal $\delta^{18}O_p$ show larger variability during the May–November (MJJASON, pale green) wet season compared to the December–April (DJFMA, red) dry period. (**b**) Daily and monthly climate data at Cobán and $\delta^{18}O_p$ during the study period. From top: relative humidity (%), surface temperature (°C), $\delta^{18}O_p$ (‰ VSMOW), and rainfall amount (mm). Monthly averages are shown in bold. Amount-weighted monthly $\delta^{18}O_p$ is shown in black line. Y-axis for $\delta^{18}O_p$ is plotted in reverse. Grey shading bars highlight wet season months. *Data source*: INSIVUMEH station at Cobán airport (see Sect. "Methods" for details).

The LMWL slope (8.2) is nearly identical to the slope defined by the Global Meteoric Water Line (GMWL)[12]. Given the strong δ^{18}O-δD relationship, our discussion will focus primarily on δ^{18}O.

The Cobán hydroclimate is markedly seasonal, consisting of a wet summer season from May through November (MJJASON) and a relatively dry winter from December to April (DJFMA), with mean annual rainfall of ~ 2500 mm[48] (Fig. 1). These seasonal regimes reflect the interplay between latitudinal migrations of the ITCZ, thermal conditions of the nearby ocean basins (Caribbean Sea-Tropical North Atlantic, Gulf of Mexico, and Eastern Tropical Pacific), and surface wind dynamics and their interaction with local topography[49–54]. About 75% of the annual total precipitation is concentrated during the wet season (Fig. S1a), coinciding with

warmer regional SSTs (> 27.5 °C), a northern position of the tropical rainbelt, and weaker easterly winds, which promote deeper regional atmospheric convection, and increased moisture advection to our study site[53,55]. The wet season is interrupted by a period of reduced precipitation during July–August, known as the Mid-Summer Drought, in which steeper zonal pressure gradients within the Caribbean region linked to westward expansion of the North Atlantic Subtropical High (NASH), strengthen the Caribbean Low-Level Jets (CLLJs) and increase atmospheric subsidence, suppressing regional convection[56–59]. The late wet season features a marked increase in tropical cyclones, contributing to a second rainfall maxima between September-October[60]. In contrast, winter precipitation is typically associated with more localized, weaker and shallow convection, and sporadic extratropical cold surges[61].

We observe a marked seasonal signal in the $\delta^{18}O_p$ data, with more negative values during the wet season relative to the winter months (Fig. 2b), despite winter months in our study period (2021–2023) being anomalously wet compared to the long-term (1980–2018) mean climatology (Fig. S1b). Average MJJASON $\delta^{18}O_p$ is − 5.54 ± 3.8 (1σ) ‰, while DJFMA mean $\delta^{18}O_p$ is -1.7 ± 1.4 (1σ) ‰. Notably, lower $\delta^{18}O_p$ values are observed in the early (May–June) and late (September–October) wet season, bracketing a slight $\delta^{18}O_p$ increase during the Mid-Summer Drought in July–August (Fig. 2b).

To test for a local amount effect, we correlated daily $\delta^{18}O_p$ with local rainfall amount, and the two, while significant, are only weakly correlated ($R^2 = 0.05$, $p < 0.01$; Fig. 3a), suggesting that intensity of individual local rainfall events has limited influence on $\delta^{18}O_p$. The correlation becomes slightly higher during the MJJASON wet season ($R^2 = 0.12$, $p < 0.01$; not shown), consistently with increased frequency and amount of daily precipitation. To test for a larger-scale potential forcing, we document a much stronger relationship between Cobán daily $\delta^{18}O_p$ and spatially-integrated (3° × 3° latitude–longitude bounding box) regional rainfall amount[62] ($R^2 = 0.44$, $p < 0.01$; Fig. 3b), indicating that regional-scale atmospheric processes exert larger influence on rainfall isotope variability. This relationship becomes even stronger when regional rainfall is integrated over 2-to-5 days prior to sampling date (maximum correlation at t-2; Fig. S4a), suggesting that $\delta^{18}O_p$ at Cobán reflects rainfall processes integrated over a 2–5-day timescale. Hence, even small or moderate rainfall events at the site can yield low $\delta^{18}O_p$ values if airmasses have undergone larger upstream isotopic depletion following rainfall events prior to the sampling date. This temporal and spatial integration of $\delta^{18}O_p$ is more strongly evidenced at monthly timescales, where both regional and local amount effect become much more pronounced (Fig. 3c–d). The lower amount-weighted monthly $\delta^{18}O_p$ values during MJJASON are consistent with enhanced regional precipitation during the monsoon wet season, whereby more pronounced integrated airmass isotopic depletion is associated with organized deep convection.

Moisture source changes and upstream airmass rainout effect on $\delta^{18}O_p$

To test the relationship between upstream airmass rainout, moisture dynamics and $\delta^{18}O_p$ variability, we analyzed the history of airmasses contributing to rainfall at Cobán during our study interval (Fig. S5–S6). Previous studies have shown the changes in moisture source regions and transport dynamics can exert a strong influence on $\delta^{18}O_p$[63–65]. In the southern Central American Isthmus, seasonal shifts from predominantly Caribbean to Eastern Tropical Pacific moisture were linked to the latitudinal migration of the ITCZ and surface wind convergence over the Isthmus[43,66].

We evaluated moisture uptake regions in air masses five days prior to the rainfall events at Cobán (see Sect. "Methods"). Five major source regions were identified, in agreement with previous regional studies[36,67,68]: Caribbean-Atlantic (CarAtl), Gulf of Mexico (GoM), Eastern Pacific (EPac), and the Mesoamerican (MAC) and North American (NAC) continents (Fig. 4). The largest moisture supply to rainfall at Cobán is from the

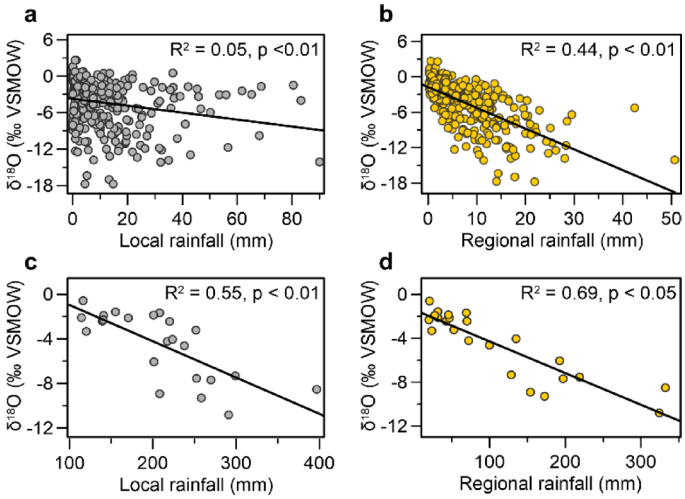


Fig. 3. Amount effect on $\delta^{18}O_p$ in Guatemala. Local and regional rainfall amount versus daily (**a–b**) and amount-weighted monthly average (**c–d**) $\delta^{18}O_p$ at Cobán. The stronger correlation with regional precipitation supports a strong regional atmospheric control on Guatemalan $\delta^{18}O_p$ composition. Regional rainfall data are spatially-averaged between 88 and 91°W and 14–17°N from NASA GPM-IMERG V07 gridded data.

CarAtl region, accounting for ~ 55% of total moisture contribution during the study interval. Notably, the second most important source is the MAC region (~ 21%), suggesting that continental moisture recycling (i.e., evapotranspiration) is an important component of the regional water budget[68]. The GoM and EPac regions contribute respectively ~ 14% and 7% of total, while moisture supply from the NAC is substantially small (3%; Fig. S7a).

To investigate the effects of changes in source regions on $\delta^{18}O_p$, we analyzed temporal variations of $\delta^{18}O_p$ during days when a single region accounted for over 60% of total moisture uptake along the airmass trajectory (see Sect. "Methods"). Moisture sourced from CarAtl region (amount-weighted -5.1‰ VSMOW) is persistent year-round and exhibits marked variability with the lowest values during MJJASON (Fig. 4, Fig. S7b). A slight increase in CarAtl-sourced $\delta^{18}O_p$ is observed coevally to decreased cumulative rainfall along trajectory during July–August, consistent with a broader decrease in regional precipitation associated with the Mid-Summer Drought (MSD in Fig. 4c). During the dry season (DJFMA), CarAtl sourced rainfall shows heavier isotopic values, associated with substantial decrease in upstream rainfall. Despite near-similar cumulative rainfall to winter months, July $\delta^{18}O_p$ values remain more negative than dry season values because regional atmospheric convection, while weakened during the Mid-Summer Drought, remains active compared to winter months, maintaining upstream isotopic depletion (i.e., via moisture advection) regardless of month-to-month upstream precipitation variability. Moisture originating from the Eastern Pacific Ocean contributes mostly during the dry-to-wet transition (Apr-June), whereas continental moisture from the Mesoamerican region increases during the early (June) and late (September) wet season. Both EPac and MAC-sourced $\delta^{18}O_p$ feature more negative amount-weighted average $\delta^{18}O_p$ (− 8.1‰ and − 6.7‰, respectively), and larger variability than moisture sourced from CarAtl (Fig. S7b). $\delta^{18}O_p$ values from both regions show stronger correlation with upstream cumulative rainfall along trajectory, consistent with a strong airmass rainout effect (Fig. 4c and Fig. S8). In contrast, GoM-sourced moisture occurred mostly during the wet-to-dry season transition and throughout the winter months and exhibits the least negative $\delta^{18}O_p$ values and lowest variability (amount-weighted − 3.8 ‰).

The high $\delta^{18}O_p$ variability observed within each source region, rather than between source regions, points to a dominant role of source-to-site atmospheric processes in controlling $\delta^{18}O_p$ at Cobán, independent of moisture origin. For example, CarAtl-sourced rainfall during the winter dry season is associated with reduced upstream rainout and lower regional rainfall amount, whereas during the wet season, enhanced regional precipitation and upstream rainout linked to deeper regional convection, promotes heavy isotope depletion within the airmasses reaching Cobán (Fig. 4c and Figs. S8–S9). The lowest $\delta^{18}O_p$ values from EPac-sourced rainfall are consistent with increased rainout as airmasses traverse the high Central American cordilleras and enhanced regional

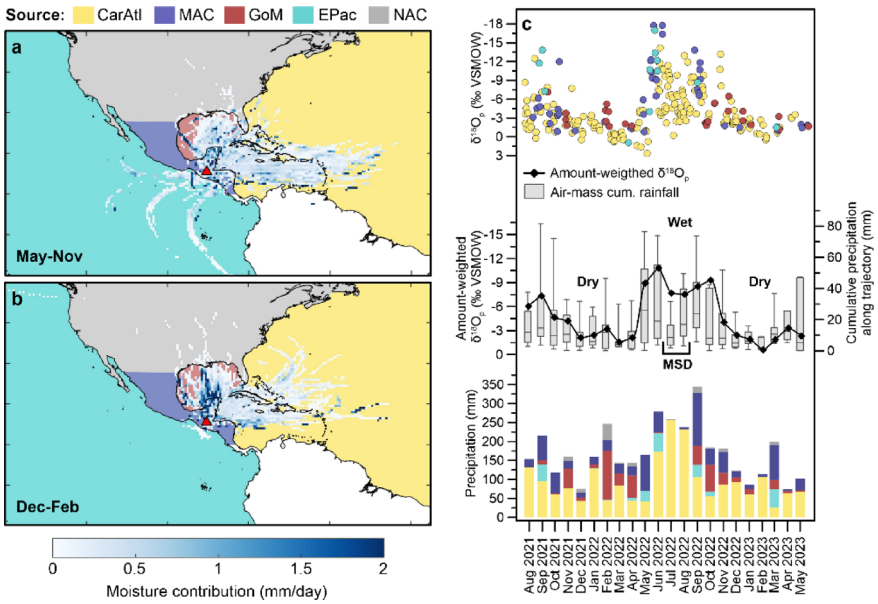


Fig. 4. Moisture source and airmass rainout influence on Guatemalan $\delta^{18}O_p$. Moisture contribution to rainfall at Cobán (mm/day) from 120 h air-mass trajectories for the interval August 2021 to May 2023, grouped by season: (**a**) May–November (MJJASON) and (**b**) December–April (DJFMA). Values are averages of all uptakes at each grid cell (0.5° × 0.5°). Colored areas represent main source regions: Caribbean-Atlantic Ocean (CarAtl; yellow), Eastern Pacific (EPac; cyan), Gulf of Mexico (GoM; red), Mesoamerican continent (MAC; blue), and North American continent (NAC; grey; see Sect. "Methods"). (**c**) Comparison between Cobán rainfall $\delta^{18}O_p$, cumulative rainfall along trajectory, and regional moisture contribution. From the top: $\delta^{18}O_p$ values for their respective dominant source regions color-coded by main source area (n = 269; see Sect. "Methods"), box-and-whisker plot of cumulative monthly rainfall along trajectory and amount-weighted monthly mean $\delta^{18}O_p$ (black diamonds and line), and fractional moisture contribution of each source region to monthly rainfall at Cobán. The Mid-Summer Drought (MSD) during July–August is noted. Boxes represent 1st and 3rd quartiles; whiskers define the 5th and 95th percentiles; line is the median.

precipitation amount (Figs. S8 and S9), influenced by the northern position of the eastern tropical Pacific ITCZ at the onset of the wet season[69,70]. In contrast, the higher amount weighted $\delta^{18}O_p$ values of GoM-sourced rainfall is consistent with generally weaker regional rainfall and reduced upstream rainout (Fig. S8 and S9), leading to less heavy isotope depletion of airmasses reaching Cobán during the dry season (Fig. S4c), where precipitation mostly consists of shallow, isolated convection and /or orographic rainfall linked to extratropical cold surges[61].

To quantitatively test moisture source effects on Coban seasonal $\delta^{18}O_p$, we modeled monthly $\delta^{18}O_p$ using source-specific amount-weighted mean $\delta^{18}O_p$ signatures (Fig. S7b) weighted by the fractional contribution of each source region to monthly rainfall at Cobán (Fig. S10). The source-based reconstruction does not reproduce the observed seasonal $\delta^{18}O_p$ variability. While the reconstruction captures a slight $\delta^{18}O_p$ decrease (~1‰) during wet months—consistent with the increased fractional contribution of the more isotopically depleted CarAtl, EPac and MAC regions—the overall reconstructed variability (~2‰) is substantially smaller than the observed ~10‰ seasonal range. This systematic underestimate of observed amplitude demonstrates that shifts in moisture source fractional contribution alone cannot explain $\delta^{18}O_p$ variability at Cobán, confirming that source-to-site atmospheric processes, and particularly upstream airmass rainout history and regional precipitation amount effects, are more important controls on rainfall isotopic variability.

We further compare deuterium excess (d-ex; $\delta^2H - 8*\delta^{18}O$)[4] of precipitation sourced from each region with relative humidity (RH) at the uptake region. Generally, d-ex for ocean-sourced rain days exhibits robust correlation with source RH (Fig. S11), indicating a strong influence of boundary layers conditions during water vapor formation. Rainfall sourced from the Gulf of Mexico has higher median values compared to other source regions (Fig. S7c). We suggest that the isotopic composition of northerly airmasses reaching Cobán during the dry winter season—when the GoM source is more prominent—is influenced by enhanced kinetic fractionation at the source, possibly from evaporation in a drier boundary layer and/or larger ocean–atmosphere temperature gradients, consistent with the higher correlation between uptake RH and d-ex in GoM dominated samples (Fig. S11). Our findings are also consistent with studies reporting higher d-ex values in GoM-sourced rainfall over North America[71,72]. Notably, MAC-sourced moisture rainfall exhibits d-ex values statistically similar to the rainfall sourced from the Caribbean and eastern Pacific (Fig S4c) and a weak, non-significant deuterium excess relationship with RH conditions at the uptake source locations (Fig. S11), suggesting that continental moisture recycling is mostly dominated by plant (evapo)transpiration[31,73] during the early and late wet season rainfall maxima rather than bare soil evaporation, which would enhance evaporative kinetic processes and increase d-excess[31]. This interpretation is consistent with studies supporting the influence of plant transpiration on tropical rainfall patterns[74–76]. Future water tagging experiments and analysis of triple oxygen isotopes, particularly ^{17}O-excess ($\Delta'^{17}O$)[77,78], will further allow to quantify between the relative contribution of soil evaporation and plant transpiration to rainfall in northern Central America.

Overall, our back-trajectory moisture analysis and source-based $\delta^{18}O_p$ reconstruction, along with source-specific d-excess, strongly suggest that the distinct rainfall isotopic signatures between seasons at Cobán are largely decoupled from changes in moisture source region alone, and instead are primarily driven by seasonal changes in source-to-site atmospheric processes.

Regional-scale organized convection control on $\delta^{18}O_p$ variability

Several studies concluded that tropical rain type (convective vs. stratiform[79]) is a dominant factor controlling $\delta^{18}O_p$ variability[20–22,45], based on the strong correlation between $\delta^{18}O_p$ and stratiform rain fraction documented at many tropical sites, including the southern Central American Isthmus[21,45]. Convective rainfall is characterized by strong vertical air motion and higher precipitation intensity, and can occur as large-scale organized and/or mesoscale convective systems (MCS) or as isolated, shallow cloud cells (mostly cumulus and cumulonimbus)[80]. In contrast, stratiform rainfall is typically associated with weaker vertical motion and lower-intensity rainfall[81], and mostly develops from the decay of older convective systems or co-existing with deep, active convective cells within large-scale or mesoscale convective complexes[80,82]. Within this framework, lower $\delta^{18}O_p$ values have been associated with a higher fraction of stratiform rain, while higher $\delta^{18}O_p$ values were linked to larger proportion of convective rain[20,41], whilst the physical mechanisms underlying these differences remain largely disputed[20,23,24,83,84].

Over two-thirds of mean annual rainfall occurring during the wet monsoon season in northern Central America is associated with the large-scale organized, deep convective systems, in which convective and stratiform rainfall often coexist[50,85]. Hence, we focus on the relationship between regional-scale convective activity and stratiform rain fraction and their effects on $\delta^{18}O_p$ variability, rather than on the distinct isotopic signature of convective and stratiform rain type. We compare stratiform rain fraction (F_{st}) and outgoing longwave radiation (OLR)—a measure of cold top-cloudiness widely applied as a proxy for regional deep convection[29,82,86–89]—from satellite data (see Sect. "Methods") with daily and monthly $\delta^{18}O_p$ values at Cobán. Generally, lower OLR values (< 220 W/m^2) indicate higher cloud energy absorption, reflecting colder top-clouds, and more vigorous/deeper convection[88,90]. We find a strong co-variation between changes in regional-scale organized convection, stratiform rain fraction and $\delta^{18}O$ variability (Fig. 5). Lower OLR (deeper convection) over the regional domain encompassing our study site is associated with higher proportion of stratiform rain and lower $\delta^{18}O_p$ values. Conversely, more positive $\delta^{18}O_p$ are coupled to higher OLR and reduced F_{st}. The strong and significant correlation between $\delta^{18}O_p$ and OLR observed at both daily ($R^2 = 0.60$, $p < 0.01$; Fig. 5a) and monthly ($R^2 = 0.83$, $p < 0.01$; Fig. 5d) scales suggests that variations in $\delta^{18}O_p$ at Cobán capture regional-scale changes in the broader atmospheric convective activity. We also observed significant correlations between Cobán $\delta^{18}O_p$ and F_{st} ($R^2 = 0.30$, $p < 0.01$ for daily; $R^2 = 0.61$, $p < 0.05$; Fig. 5b and d, respectively), supporting a link between stratiform rain fraction and $\delta^{18}O_p$ variability, in agreement with other tropical isotopic studies[21,45]. Our data show that regional-scale convective activity is the dominant control on $\delta^{18}O_p$, with a secondary control by stratiform rain fraction. The robust linear relationship between OLR, F_{st}, and $\delta^{18}O_p$ further supports the primary role of

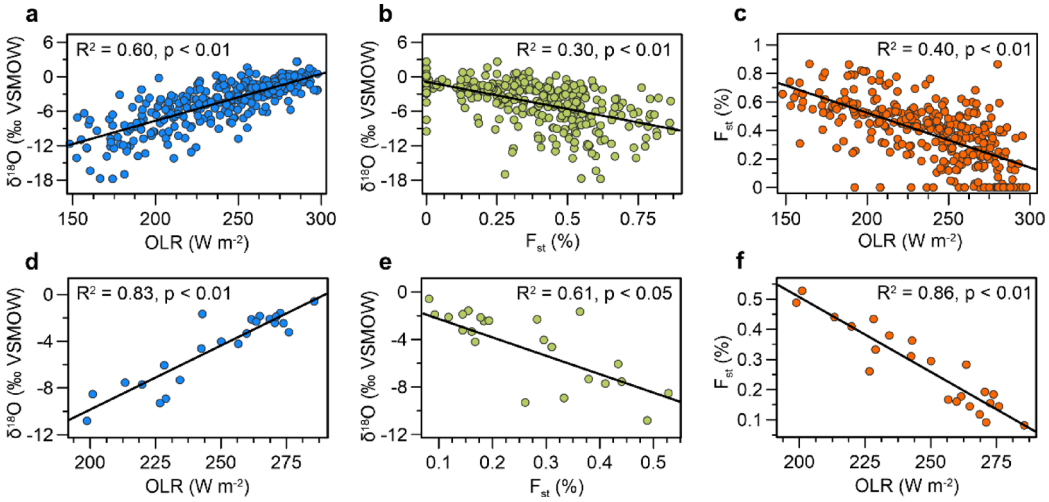


Fig. 5. Influence of regional-scale convective activity and stratiform rain fraction on Guatemalan $\delta^{18}O_p$ Correlation between Cobán $\delta^{18}O_p$, outgoing longwave radiation (OLR), and stratiform fraction (F_{st}) for daily (**a–c**) and monthly (**d–f**) timescales. OLR and stratiform fraction data are spatially-averaged between 88–91°W and 14–17°N. Correlation are for n = 335; all p-values are adjusted for effective degree of freedom (N_{eff}). See Supplementary Table 1–2. Data source: ERA5 (OLR) and GPM DPR 2AKu (F_{st}).

organized deep convection in modulating rainfall isotope variability. Most importantly, our findings underscore that the influence of stratiform rain fraction on $\delta^{18}O_p$ is closely linked to strength and organization of regional convective systems, rather than an independent control on isotopic composition.

Previous studies have extensively discussed the multiple mechanisms driving heavy isotopic depletion within organized convective systems[24,25,91–94]. Most theoretical and observational studies agree that increasing cloud-top altitude within deep convective core cells enhances net condensation and heavy isotope depletion through rainout. As the convective systems develop, isotopically-depleted water vapor from the downdraft is recycled in the updraft region at the sub-cloud layer within the convective core cells. Thus, increasing strength/depth of convection intensifies heavy isotope distillation, resulting in isotopically light water vapor supply to subsequent precipitation[25,92]. Within large-scale and mesoscale convective systems characterized by a large stratiform rain area, low-$\delta^{18}O$ water vapor from the convective core region is advected into the stratiform region at mid-high tropospheric levels, imprinting lower $\delta^{18}O$ signatures to the $\delta^{18}O_p$ of the stratiform rain area[23,91].Hydrometeor growth within the stratiform region by aggregation of low-$\delta^{18}O$ tropospheric water vapor[20] further contributes to $\delta^{18}O_p$ decrease. While our study does not aim to solve the ongoing debate about the role of stratiform and convective rain type in modulating $\delta^{18}O_p$ across the tropics[20,23,83], our findings suggest that at our study site the prior-convective isotopic imprinting-effect[23] and low-$\delta^{18}O$ tropospheric hydrometeor aggregation in stratiform regions[20] are not mutually exclusive, and both contribute to explain heavy rainfall isotopic depletion within large-scale, organized deep convective systems (i.e., during the wet monsoon season). Thus, we propose that $\delta^{18}O_p$ variations in northern Central America are driven by the strength of organized deep convection and, consequently, by the changes in stratiform rain proportion. These results are consistent with observations and modeling studies across the tropics suggesting that within large scale-convective systems, moisture in stratiform regions is primarily inherited from earlier or coeval convective core cells, and that further isotopic depletion within the stratiform area through tropospheric water vapor aggregation results in lower $\delta^{18}O_p$ at the surface[23,24,84,89,91,92,94].

We also found a strong positive correlation between $\delta^{18}O_p$ and OLR in rainfall sourced from each of the source regions (EPac, MAC, and CarAtl), and a weak correlation with GoM-sourced rainfall (Fig. S12), consistent with the marked seasonality of convective activity in the region. Thus, more negative $\delta^{18}O_p$ values coincide with increasing wet-season large-scale, organized convective activity and larger rainout of airmasses originating mostly from CarAtl, EPac and MAC regions, while weaker, localized convection is associated with isotopically heavier rainfall originating from the GoM and CarAtl regions during the winter season.

Our interpretation of a regionally-integrated signal recorded in Guatemalan rainfall isotopes is supported by the strong spatial coherence between Cobán $\delta^{18}O_p$, OLR and rainfall gridded data (Fig. 6). On daily timescales, both OLR and rainfall integrated over 2–3 days prior to rainfall measurement at Cobán exhibit the strongest correlation with $\delta^{18}O_p$, extending broadly across the Caribbean Sea, Gulf of Mexico and Central American landmass (Fig. 6A and B), supporting that upstream organized convective activity and regional precipitation contribute to moisture ^{18}O depletion delivered to our study site.

To further evaluate the spatial and temporal persistence of these regional atmospheric controls on $\delta^{18}O_p$ beyond our 2021–2023 study interval, we integrate our measurements with model-based $\delta^{18}O_p$ from IsoGSM4[47], an isotope-enabled general circulation model with ~ 50 km horizontal resolution that incorporates water isotopes within the ocean, atmosphere and land, allowing robust analysis of regional hydrologic processes within heterogeneous terrains such as Central America. IsoGSM4 data spatially-averaged over both local (2

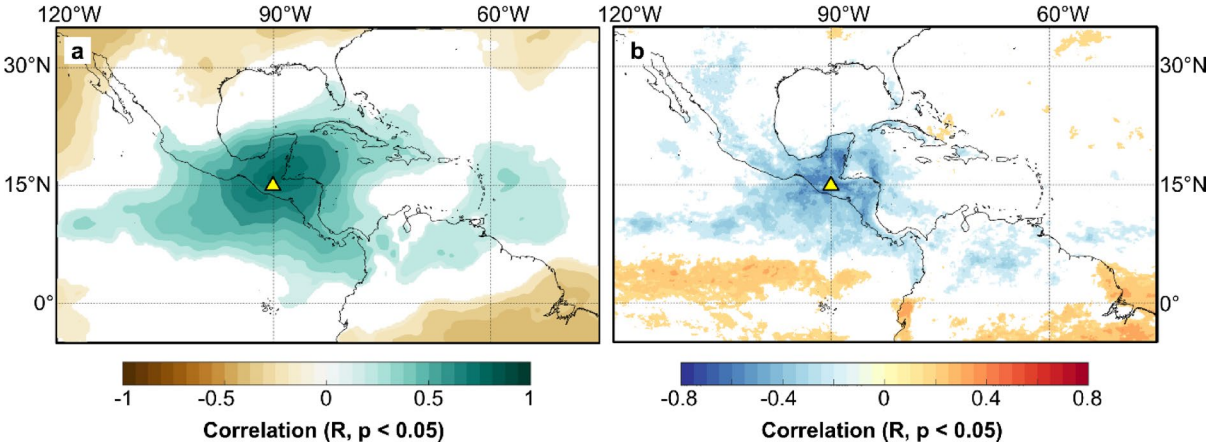


Fig. 6. Spatial correlation maps of measured $\delta^{18}O_p$ and gridded OLR and rainfall data. (**a**) Correlation between Cobán daily $\delta^{18}O_p$ and OLR averaged over two days prior to sampling date for the 2021–2023 study interval; (**b**) Correlation between daily $\delta^{18}O_p$ and integrated-rainfall over three days prior to rainfall day; Only significant correlation ($p < 0.05$) is shown. The yellow triangle in (**a** and **b**) shows Cobán location.*Data source*: ERA5 (OLR), GPM-IMERG V07 (rainfall).

grid cells centered at Cobán) and regional (14–17°N, 88–92°W) domains were evaluated against our daily and monthly $\delta^{18}O_p$ data (Fig. S13; see Sect. "Methods"). We found a stronger correlation for the regionally-averaged domain ($R^2 = 0.65$, $p < 0.01$) than for the local domain ($R^2 = 0.41$, $p < 0.01$), consistent with our interpretation that $\delta^{18}O_p$ variability at Cobán is influenced by broader regional-scale hydroclimatic processes. We therefore use the regionally-averaged IsoGSM4 $\delta^{18}O_p$ to test the spatial relationship over a broader temporal interval (1998–2024; Fig. 7). The IsoGSM4-based spatial correlations over the 1998–2024 period show that atmospheric convection and regional precipitation controls on $\delta^{18}O_p$ persist beyond our 2021–2023 study interval, suggesting that the regional convective and rainout controls on $\delta^{18}O_p$ are persistent features of the regional hydroclimate across multiple timescales, from daily to interannual. Further, IsoGSM4 regional $\delta^{18}O_p$ fields also reveal a pronounced seasonal contrast in the spatial pattern of isotopic variability across the broader Central American and Caribbean region (Fig. S14). Most importantly, during the wet monsoon season the modeled monthly $\delta^{18}O_p$ exhibits coherent and significant spatial correlations with OLR, vertically-integrated moisture flux convergence (VIMFC), and precipitation amount across Central America and the broader upstream Caribbean domain. Contrarily, no clear and/or coherent correlation is observed between $\delta^{18}O_p$ and regional climate variables (except OLR) during the dry season, consistent with more localized convective rainfall and the lack of large-scale, organized convective systems (Fig. 7).

During the wet season, more intense and organized convective systems develop over and upstream of our study site, linked to warmer regional SSTs within the AWP and a northern shift of the tropical rainbelt[53,55,95]. Weakening of the zonal trade winds and reduced atmospheric stability over the Caribbean favor the development of large-scale organized convective systems, increasing moisture flux convergence over Central America (Fig. S14-S15). The resulting increase in deep convective activity contributes to the inverse relationship between $\delta^{18}O_p$ values and more intense regional precipitation[25,91] (Fig. 7). In contrast, dry season rainfall at Cobán is typically associated with shallow convection and exhibits higher $\delta^{18}O_p$ values (Fig. S14b). As previous studies have shown[24,92], net condensation in isolated, shallow convective clouds occurs at lower tropospheric levels and results in less heavy isotope distillation and less negative $\delta^{18}O_p$ values. Most winter months within our study interval show precipitation amounts exceeding the climatological mean (1980–2018; Fig. S1b), suggesting that, despite increased frequency, the weaker intensity of shallow convective rainfall—relative to wet season large-scale deep convective systems—was associated with reduced airmass heavy isotope depletion and higher $\delta^{18}O_p$ values at Cobán, confirming that convective intensity rather than local rainfall amount drives the isotopic seasonal signal.

Summary and implications for isotope-based paleoclimate reconstructions

Our analysis of rainfall isotopes from Guatemala provides key insights into the regional hydroclimatic controls on $\delta^{18}O_p$ variability in northern Central America. We identify a strong seasonal pattern in our daily $\delta^{18}O_p$ data that is not explained by changes in local rainfall amount. Instead, $\delta^{18}O_p$ variability is more strongly associated with regional atmospheric processes, primarily regional-scale, organized deep convection and upstream rainout processes. IsoGSM4 model-based isotope data further support our interpretations, showing that the relationship between large-scale atmospheric convection, regional precipitation amount, and $\delta^{18}O_p$ is persistent on multiple timescales, from daily to interannual. Further, our study shows that the application of high-resolution isotope-enabled climate models like IsoGSM4[47] provides useful tools to complement site-specific isotope observations and test for regional hydroclimate dynamics, particularly for regions where rainfall isotope data are spatially scarce.

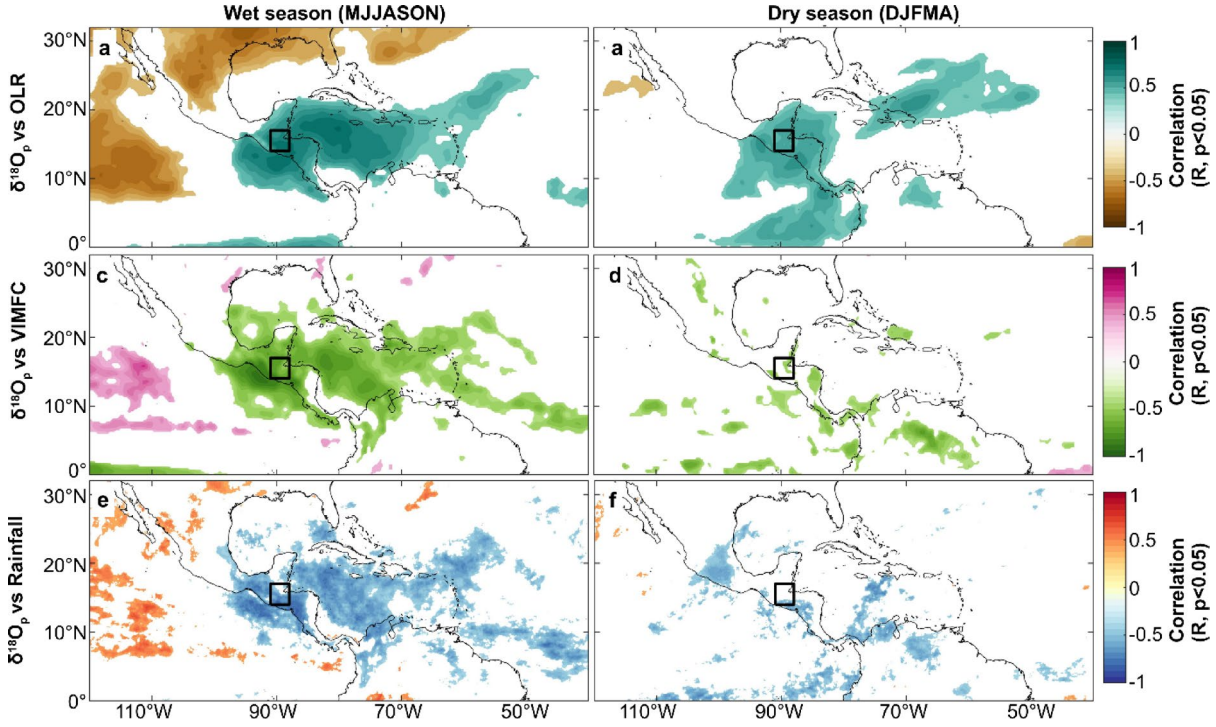


Fig. 7. Spatial correlation maps of IsoGSM4 amount-weighted $\delta^{18}O_p$ (‰ VSMOW, averaged over the black square area) and gridded ERA5 outgoing longwave radiation (OLR, W m^{-2}, **a**–**b**), ERA5 vertically integrated moisture flux convergence (VIMFC, kg m^{-2} s^{-1}, **c**–**d**), and IMERG rainfall (mm/day, **e**–**f**) for the wet (left) and dry season (right). The coherent spatial patterns observed among all variables during the MJJASON suggest larger influence of wet season atmospheric processes on Guatemalan rainfall isotopes. Enhanced moisture convergence to Central America during MJJASON is coupled with stronger regional atmospheric convection (lower OLR) and higher rainfall amount over and upstream our study area, contributing to larger airmass ^{18}O depletion and lower $\delta^{18}O_p$ values at our study area (black square). White area represents region of non-significant correlation ($p > 0.05$).

Taken together, our findings indicate that rainfall isotopes in northern Central America reflect a regionally-integrated hydroclimatic signal that is modulated by strength and organization of convective systems and upstream source-to-site precipitation amount. Further, the persistent seasonal $\delta^{18}O_p$ signal observed on multiple timescales suggest that $\delta^{18}O_p$ is largely dominated by regional monsoon convective variability. We thus posit that isotope-based paleoclimate archives recording variations in $\delta^{18}O_p$ (or δD), such as speleothems, leaf-waxes and tree rings in humid environments, as well as open-system lake records from northern Central America can be interpreted as proxies of regional hydroclimate dynamics and changes in the broader monsoon convection. The addition of moisture-sensitive proxies beyond oxygen and hydrogen stable isotopes can help to confirm the coupling of regional to local hydroclimates[96,97]. Furthermore, because of the unique d-ex values of rainfall sourced from the Gulf of Mexico and the significant moisture contribution from the Mesoamerican continent to our study area, speleothems may also hold promise for $\Delta'^{17}O$ analysis as a paleo-moisture source proxy[98,99]. Our study thus underscores the importance of applying stable isotopes to understand the links between regional and local climate dynamics to improve interpretations of regional paleo-proxy records, and further highlights the need for expanding isotope monitoring networks in understudied regions like northern Central America, where the impacts of climate change are already affecting millions of people.

Methods

Rainwater sampling and isotopic analysis

Daily rainfall was collected in the city of Cobán, Alta Verapaz Department, Guatemala (15.47°N, 90.38°W) from July 20, 2021 to May 28, 2023 using a passive rain collector (Palmex RS1, Zagreb, Croatia). No rainfall volume was measured at the sampling site. Rainwaters were filtered in the lab using 0.45 µm nylon filters, transferred to HDPE 30 ml bottles, tape-sealed and stored at temperature of ~ 4 °C until analysis to prevent post-sampling evaporation. Isotope measurements were made at the Las Vegas Isotope Science Laboratory (LVIS) of the University of Nevada Las Vegas and at the Center for Stable Isotopes (CSI) of the University of New Mexico (Albuquerque, NM). Rainfall collected between July 2021 and July 2022 were analyzed at the CSI-UNM laboratory facilities using a cavity-ring down spectroscopy Picarro L1102-I Water Isotopic Analyzer, and samples from August 2022 to May 2023 were measured at the UNLV-LVIS laboratory using a Picarro L2140-i water isotope analyzer. Unknown sample values were bracketed with internal standards calibrated to international standard scale VSMOW-SLAP. Cross-laboratory measurements were performed to further test

replicability analysis between laboratories and yielded virtually identical isotopic values. Data are reported as δ-values relative to VSMOW in ‰. Analytical precision is 0.1–0.2 ‰ for $\delta^{18}O$ and 0.5–0.8 ‰ for $\delta^{2}H$.

Data collection

Daily data of surface temperature, rainfall amount, and relative humidity were obtained from the meteorological station of the Instituto Nacional de Sismología, Vulcanología, Meteorología e Hidrología (INSIVUMEH) at the Cobán airport, approximately 5 km from our rainfall sampling site. Gridded precipitation data (0.1° × 0.1°spatial resolution) were acquired from the NASA Global Precipitation Measurement (GPM) IMERG V07 at hourly (GPM_3IMERGHH), daily (GPM_3IMERGDF), and monthly (GPM_3IMERGM) timescales[62]. Outgoing longwave radiation (OLR), defined as the top of the atmosphere cold cloudiness related to the depth and height of convective clouds, was used as a proxy for regional convective strength. OLR data were calculated at hourly, daily, and monthly scales from the mean top net longwave radiation flux data obtained from the ECMWF Reanalysis v5 (ERA5) data (0.25° × 0.25° spatial resolution). Calculated daily and monthly ERA5 OLR were evaluated against OLR data from the University of Maryland Climate Data Record (UMD CDR, http://olr.umd.edu/)[100,101], respectively having 1° × 1° and 2.5° × 2.5° spatial resolution (Fig. S16). Vertically-integrated moisture flux convergence (VIMFC) was calculated as the negative of moisture flux divergence gridded data, obtained from the ECMWF Reanalysis v5 (ERA5) data (0.25° × 0.25° spatial resolution) for the 1998–2024 period. Daily stratiform rain fraction (F_{st}) data were obtained from the Ku Band precipitation profile of the NASA GPM Dual-Frequency Precipitation Radar (DPR) Level 2A product[102] The DPR satellite has a swath width (horizontal coverage) of 245 km, and orbits at an altitude of 407 km and a 65-degree inclination, requiring approximately 10 days and 164 orbits to cover the entire equatorial region[21,102]. Therefore, daily stratiform fraction data were not available for all precipitation days during our study interval. To address this limitation, we estimated F_{st} for days with no satellite coverage based on the relationship between area-averaged precipitation amount and F_{st}, following Munksgaard, et al.[21] and Sánchez-Murillo, et al.[45]. In the tropics, stratiform rainfall is generally associated with larger rain area compared to convective rainfall[103]. Thus, higher F_{st} likely results in higher area averaged rainfall amount[21,103,104]. We found a strong logarithmic relationship between area averaged daily rainfall amount and F_{st} over the 3° × 3° domain (14–17°N, 88–91°W) encompassing our study site for the period 2018–2025, extending beyond our study interval to sample size and improve regression robustness (Fig. S17), and applied this regression to estimate F_{st} for the missing days during our 2021–2023 study interval. Rainfall, OLR, and F_{st} data were all extracted within the same 3° × 3° domain (14–17°N, 88–91°W) and spatially-averaged prior to correlation analysis. Modeled $\delta^{18}O_p$ data were retrieved from the Isotope-incorporated General Spectral Model Version 4 (IsoGSM4)[47], publicly available upon author request at https://zenodo.org/records/14676105. IsoGSM4 is the latest high-resolution (~ 50 km) implementation of the IsoGSM model family[105,106], nudged to the 25 km ERA5 reanalysis data, providing significant advance in reproducing regional climate processes, including for regions with highly heterogeneous terrains (i.e., Central America). We extracted daily and monthly $\delta^{18}O_p$ data from two spatial domains, local (2-grid cell spatial scale centered at Cobán) and regional (3° × 3° bounding box, 14–17°N, 88–91°W) and compared with our $\delta^{18}O_p$ measured at Cobán (Fig. S13).Only IsoGSM4 daily data with precipitation > 0.1 mm/day (Filtered_0.1_mm_per_day) were used to reduce numerical noise associated with small precipitation rates[47]. Overall, IsoGSM4 data reproduce our $\delta^{18}O_p$ values quite well. However, we found a stronger correlation between measured $\delta^{18}O_p$ and regionally-averaged IsoGSM4 $\delta^{18}O_p$ ($R^2 = 0.65$, $p < 0.01$) compared to local ($R^2 = 0.40$, $p < 0.01$), supporting a stronger regionally-integrated component of Coban $\delta^{18}O_p$. Therefore, we retrieved IsoGSM4 amount-weighted monthly $\delta^{18}O_p$ from the regional domain for the period 1998–2024 and compared with OLR, VIMFC, rainfall data.

Air-mass trajectories and moisture uptake analysis

To examine moisture history reaching Cobán throughout the sampling period (July 2021-May 2023), air-mass trajectories for each rainfall date (n = 335 days) were modeled using Pysplit[107,108], a Python-based interface of the NOAA's Air Resources Laboratory (ARL) Hybrid Single-Particle Lagrangian Integrated Trajectory (HYSPLIT) model[109]. Trajectories were initiated from the sampling site (15.47°N, 90.38°W) at an elevation of 1500 m above ground level (m agl), and run 120-h backwards (5 days prior to rainfall day) four times daily (UTC-6 06, 12, 18, and 00). Lagrangian modeling studies have shown that water vapor residence time in the atmosphere varies from 2–3 days up to 15 days in some locations[110]. We selected a 5-days interval as representative of global average moisture residence time[111,112] consistently with previous regional studies[36,113], as well as to reduce uncertainty with increasing time integration. Because most atmospheric water vapor is found within the first 2000 m above ground level (m agl)[114], we selected an elevation of 1500 m agl (roughly equivalent to 850 hPa level) as the starting vertical height, in agreement with previous studies[64,115,116]. Global Data Assimilation System (GDAS1) gridded reanalysis data (downloaded at https://www.ready.noaa.gov/data/archives/gdas1/) with a horizontal resolution of 1° and 23 vertical levels were used as input for trajectory calculations. While modelled trajectories provide a general framework of air-mass motions, effective moisture uptake does not occur along the entire trajectory but only in some locations and under specific conditions[117]. We thus modeled the regions of effective moisture uptake along air-mass trajectories following the method of Sodemann, et al.[117], which has been successfully applied in numerous isotope studies[17,116,118,119]. Moisture change (Δq) within an air parcel reflects a net balance between evaporation (uptake) and precipitation (removal). We calculated changes in specific humidity (Δq, g/kg) from trajectory data at intervals of 6 h (t_n-$t_{n-6\,h}$). Locations where $\Delta q \geq 0.2$ g/kg and within the planetary boundary layer (defined as the lowest atmospheric layer directly influenced by surface processes) were selected as effective moisture uptake from surface evaporation[116,120]. Δq values that fulfilled our selection criteria were binned into a 1° × 1° gridded map. Five main source regions were identified, based on the distinct oceanic sources and to distinguish between continental and oceanic regions, in agreement with previous regional studies[36,42,68,113,121]: Caribbean-Atlantic (CarAtl), Gulf of Mexico (GoM), Eastern Pacific (EPac), Mesoamerican

continent (MAC), and North American continent (NAC). For each trajectory (d), we calculated the fractional moisture contribution (fr_j) of each source region (j) as follows:

$$fr_j\,(d,j) = \frac{\sum_{i\in R_j} \Delta q\,(i,d)}{\sum_{i=1}^{N} \Delta q\,(i,d)} \tag{1}$$

where $\Delta q(i,d)$ is the moisture uptake at grid point i on day d, R_j is the total number of grid points assigned to source region j, and N is the total number of grid points in the source region. Fractional moisture contribution from each region was then weighted for the rainfall amount at the sampling site following[32]:

$$\mathrm{Pw}_j = \frac{\sum_{d=1}^{n} P_d fr_j}{\sum_{d=1}^{n} P_d} \tag{2}$$

where Pw_j is the precipitation-weighted moisture contribution (in %), n is the number of trajectories, Pd is the rainfall amount at the sampling site on day d and fr_j is the fractional moisture contribution at each grid point in each region. Daily rainfall oxygen isotope values measured at the sampling site were then assigned to a dominant source region where fractional moisture contribution from that region was > 60% of total uptake along trajectory. Based on this threshold, n = 269 $\delta^{18}O_p$ values were assignable to a dominant source region, while n = 66 $\delta^{18}O_p$ days that had multiple contributing sources regions were excluded from the analysis. Cumulative precipitation along-trajectory (CP_{trj}) was calculated for each rainy day:

$$\mathrm{CP}_{trj} = \sum_{t=0}^{t=n} P\,(t)_{xy} \tag{3}$$

where P is the rainfall amount at time t along the trajectory, while x and y are latitude and longitude, respectively. Rainfall data at x and y were extracted from the GPM_3IMERGHH hourly data.

Source-based monthly $\delta^{18}O_p$ was computed as:

$$\delta^{18}O_p\,(m) = \sum fr_j\,(m) \times \delta^{18}O_{p,j} \tag{4}$$

where $fr_j(m)$ is the monthly precipitation-weighted fractional moisture contribution of source region j for month m, and $\delta^{18}O_{p,j}$ is the source-specific amount-weighted mean isotopic signature derived from the n = 269 rainfall days assigned to a dominant source region (fractional contribution > 60%; see above; Fig. S7B); $fr_j(m)$ is defined as $S_j(m)/P(m)$, where $S_j(m)$ is the monthly precipitation amount attributed to source region j, calculated from the daily fractional contributions $fr_j(d)$ (Eq. 1) weighted by daily precipitation Pd, and $P(m)$ is the total monthly precipitation amount at Cobán. A 95% confidence interval of the monthly reconstruction was estimated using a Monte Carlo simulation (n = 10,000), in which random values within the standard error of the source-specific amount-weighted $\delta^{18}O_p$ values were selected at each iteration, and derived from the 2.5th and 97.5th percentiles (green shadow in Fig. S10).

Data treatment and statistical analysis

Correlation analysis was computed in MATLAB (MathWorks, License version 2023a). Correlation significance (p-value) was calculated accounting for data autocorrelation and adjusting for effective degree of freedom according to the method of Dawdy and Matalas[122]. A non-parametric Kruskal–Wallis test[122] was used to assess differences in d-excess median values among moisture source regions. For significant differences ($p < 0.05$), p-values were adjusted using the Dunn–Šidák pairwise post hoc method[123,124].

Data availability

Rainfall isotope data produced in the study are available in the Supplementary Data file and accessible at WaterIsotopes.org (https://wateriso.utah.edu/waterisotopes/pages/data_access/oipc.html). Mean top net longwave radiation flux data used to calculate OLR data and Vertical-integrated moisture flux convergence are accessible at https://cds.climate.copernicus.eu/datasets. OLR used to validate calculated OLR data were downloaded at UMD CDR (http://olr.umd.edu/). Precipitation and Stratiform rain fraction data were downloaded at https://disc.gsfc.nasa.gov/. Meteorological data for Hysplit back trajectory analysis were downloaded at https://www.ready.noaa.gov/data/archives/gdas1/. ISOGSM4 data are accessible (upon authors' permission) at https://zenodo.org/records/14676105. Custom MATLAB codes used for the computation of fractional moisture contribution, moisture source-based monthly δ18Op time series, and ISOGSM4 model-data validation are available from the corresponding author upon reasonable request.

Received: 31 October 2025; Accepted: 15 July 2026
Published online: 22 July 2026

References

1. Bowen, G. J., Cai, Z., Fiorella, R. P. & Putman, A. L. Isotopes in the water cycle: Regional- to global-scale patterns and applications. *Annu. Rev. Earth Planet. Sci.* **47**, 453–479. https://doi.org/10.1146/annurev-earth-053018-060220 (2019).

2. Gat, J. R. Oxygen and hydrogen isotopes in the hydrologic cycle. *Annu. Rev. Earth Planet. Sci.* **24**, 225–262. https://doi.org/10.1146/annurev.earth.24.1.225 (1996).
3. Craig, H. Isotopic variations in meteoric waters. *Science* **133**, 1702–1703 (1961).
4. Dansgaard, W. Stable isotopes in precipitation. *Tellus* **16**, 436–468. https://doi.org/10.3402/tellusa.v16i4.8993 (1964).
5. Gat, J. R. & Gonfiantini, R. Stable isotope hydrology. Deuterium and oxygen-18 in the water cycle. (1981).
6. Lachniet, M. S. Climatic and environmental controls on speleothem oxygen-isotope values. *Quat. Sci. Rev.* **28**, 412–432. https://doi.org/10.1016/j.quascirev.2008.10.021 (2009).
7. Oeschger, H. et al. Late glacial climate history from ice cores. *Clim. Process. Clim. Sensitivity* **29**, 299–306 (1984).
8. Fornace, K. L. et al. A 60,000-year record of hydrologic variability in the Central Andes from the hydrogen isotopic composition of leaf waxes in Lake Titicaca sediments. *Earth Planet. Sci. Lett.* **408**, 263–271. https://doi.org/10.1016/j.epsl.2014.10.024 (2014).
9. Nagavciuc, V., Ionita, M., Kern, Z., McCarroll, D. & Popa, I. A ~700 years perspective on the 21st century drying in the eastern part of Europe based on δ18O in tree ring cellulose. *Commun. Earth Environ.* **3**, 277. https://doi.org/10.1038/s43247-022-00605-4 (2022).
10. Galewsky, J. et al. Stable isotopes in atmospheric water vapor and applications to the hydrologic cycle. *Rev. Geophys.* **54**, 809–865. https://doi.org/10.1002/2015rg000512 (2016).
11. Konecky, B. L., Noone, D. C. & Cobb, K. M. The influence of competing hydroclimate processes on stable isotope ratios in tropical rainfall. *Geophys. Res. Lett.* **46**, 1622–1633. https://doi.org/10.1029/2018gl080188 (2019).
12. Rozanski, K., Araguás-Araguás, L. & Gonfiantini, R. Isotopic patterns in modern global precipitation. *GMS* **78**, 1–36 (1993).
13. Wang, X. et al. Hydroclimate changes across the Amazon lowlands over the past 45,000 years. *Nature* **541**, 204–207. https://doi.org/10.1038/nature20787 (2017).
14. Fleitmann, D. et al. Holocene forcing of the Indian monsoon recorded in a stalagmite from southern Oman. *Science* **300**, 1737–1739 (2003).
15. Lachniet, M. S. A 1500-year El Niño/Southern Oscillation and rainfall history for the Isthmus of Panama from speleothem calcite. *J. Geophys. Res.* https://doi.org/10.1029/2004jd004694 (2004).
16. Burns, S. J., Fleitmann, D., Matter, A., Neff, U. & Mangini, A. Speleothem evidence from Oman for continental pluvial events during interglacial periods. *Geology* **29**, 623–626 (2001).
17. Wolf, A., Roberts, W. H. G., Ersek, V., Johnson, K. R. & Griffiths, M. L. Rainwater isotopes in central Vietnam controlled by two oceanic moisture sources and rainout effects. *Sci. Rep.* **10**, 16482. https://doi.org/10.1038/s41598-020-73508-z (2020).
18. Xue, Y.-X. et al. Quantifying source effects based on rainwater δ18O from 10-year monitoring records in Southwest China. *Appl. Geochem.* **155**, 105706 (2023).
19. He, S. et al. Uncovering below cloud rain-vapor interactions during tropical rain events through simultaneous and continuous real-time monitoring of rain and vapor isotopes. *J. Geophys. Res. Atmos.* **129**, e2023JD040084 (2024).
20. Aggarwal, P. K. et al. Proportions of convective and stratiform precipitation revealed in water isotope ratios. *Nat. Geosci.* **9**, 624–629. https://doi.org/10.1038/ngeo2739 (2016).
21. Munksgaard, N. C. et al. Data descriptor: Daily observations of stable isotope ratios of rainfall in the tropics. *Sci. Rep.* **9**, 14419. https://doi.org/10.1038/s41598-019-50973-9 (2019).
22. Zwart, C. et al. The isotopic signature of monsoon conditions, cloud modes, and rainfall type. *Hydrol. Process.* **32**, 2296–2303. https://doi.org/10.1002/hyp.13140 (2018).
23. Yu, W. et al. Water isotope ratios reflect convection intensity rather than rain type proportions in the pantropics. *Sci. Adv.* **10**, eado3258. https://doi.org/10.1126/sciadv.ado3258 (2024).
24. Tharammal, T., Bala, G. & Noone, D. Impact of deep convection on the isotopic amount effect in tropical precipitation. *J. Geophys. Res. Atmos.* **122**, 1505–1523 (2017).
25. Risi, C., Bony, S. & Vimeux, F. Influence of convective processes on the isotopic composition (δ18O andδD) of precipitation and water vapor in the tropics: 2. Physical interpretation of the amount effect. *J. Geophys. Res.* https://doi.org/10.1029/2008jd009943 (2008).
26. Zwart, C., Munksgaard, N. C., Kurita, N. & Bird, M. I. Stable isotopic signature of Australian monsoon controlled by regional convection. *Quatern. Sci. Rev.* **151**, 228–235. https://doi.org/10.1016/j.quascirev.2016.09.010 (2016).
27. Zhan, Z. et al. Determining key upstream convection and rainout zones affecting δ18O in water vapor and precipitation based on 10-year continuous observations in the East Asian Monsoon region. *Earth Planet. Sci. Lett.* **601**, 117912. https://doi.org/10.1016/j.epsl.2022.117912 (2023).
28. Zhou, H. et al. Variation of δ18O in precipitation and its response to upstream atmospheric convection and rainout: A case study of Changsha station, south-central China. *Sci. Total Environ.* **659**, 1199–1208. https://doi.org/10.1016/j.scitotenv.2018.12.396 (2019).
29. Moerman, J. W. et al. Diurnal to interannual rainfall δ18O variations in northern Borneo driven by regional hydrology. *Earth Planet. Sci. Lett.* **369–370**, 108–119. https://doi.org/10.1016/j.epsl.2013.03.014 (2013).
30. Escobar, M., Hoyos, I., Nieto, R. & Villegas, J. C. The importance of continental evaporation for precipitation in Colombia: A baseline combining observations from stable isotopes and modelling moisture trajectories. *Hydrol. Process.* **36**, e14595 (2022).
31. Risi, C., Noone, D., Frankenberg, C. & Worden, J. Role of continental recycling in intraseasonal variations of continental moisture as deduced from model simulations and water vapor isotopic measurements. *Water Resour. Res.* **49**, 4136–4156. https://doi.org/10.1002/wrcr.20312 (2013).
32. Crawford, J., Hughes, C. E. & Parkes, S. D. Is the isotopic composition of event based precipitation driven by moisture source or synoptic scale weather in the Sydney Basin, Australia?. *J. Hydrol.* **507**, 213–226. https://doi.org/10.1016/j.jhydrol.2013.10.031 (2013).
33. Gou, J. et al. Relationship between precipitation isotopic compositions and synoptic atmospheric circulation patterns in the lower reach of the Yangtze River. *J. Hydrol.* **605**, 127289 (2022).
34. Lachniet, M. S. Sea surface temperature control on the stable isotopic composition of rainfall in Panama. *Geophys. Res. Lett.* https://doi.org/10.1029/2008gl036625 (2009).
35. Sánchez Murillo, R. *et al.* Spatial and temporal variation of stable isotopes in precipitation across Costa Rica: An analysis of historic GNIP records. (2013).
36. Sánchez-Murillo, R. et al. Tracing isotope precipitation patterns across Mexico. *PLoS Water* **2**, e0000136 (2023).
37. Lachniet, M. S. & Patterson, W. P. Oxygen isotope values of precipitation and surface waters in northern Central America (Belize and Guatemala) are dominated by temperature and amount effects. *Earth Planet. Sci. Lett.* **284**, 435–446. https://doi.org/10.1016/j.epsl.2009.05.010 (2009).
38. Lases-Hernandez, F., Medina-Elizalde, M., Burns, S. & Decesare, M. Long-term monitoring of drip water and groundwater stable isotopic variability in the Yucatán Peninsula: Implications for recharge and speleothem rainfall reconstruction. *Geochim. Cosmochim. Acta* **246**, 41–59. https://doi.org/10.1016/j.gca.2018.11.028 (2019).
39. Sánchez-Murillo, R. & Birkel, C. Groundwater recharge mechanisms inferred from isoscapes in a complex tropical mountainous region. *Geophys. Res. Lett.* **43**, 5060–5069. https://doi.org/10.1002/2016gl068888 (2016).
40. Sanchez-Murillo, R. et al. Isotopic composition in precipitation and groundwater in the northern mountainous region of the Central Valley of Costa Rica. *Isot. Environ. Health Stud.* **53**, 1–17. https://doi.org/10.1080/10256016.2016.1193503 (2017).
41. Sánchez-Murillo, R. et al. Tracer hydrology of the data-scarce and heterogeneous Central American Isthmus. *Hydrol. Process.* https://doi.org/10.1002/hyp.13758 (2020).

42. Bernal, J. P. et al. Variability of trace-elements and δ18O in drip water from Gruta del Rey Marcos, Guatemala; seasonal and environmental effects, and its implications for paleoclimate reconstructions. *Front. Earth Sci.* https://doi.org/10.3389/feart.2023.1112957 (2023).
43. Sánchez-Murillo, R. et al. Key drivers controlling stable isotope variations in daily precipitation of Costa Rica: Caribbean Sea versus Eastern Pacific Ocean moisture sources. *Quat. Sci. Rev.* **131**, 250–261. https://doi.org/10.1016/j.quascirev.2015.08.028 (2016).
44. Esquivel-Hernández, G. et al. Moisture transport and seasonal variations in the stable isotopic composition of rainfall in Central American and Andean Páramo during El Niño conditions (2015–2016). *Hydrol. Process.* https://doi.org/10.1002/hyp.13438 (2019).
45. Sánchez-Murillo, R. et al. Deciphering key processes controlling rainfall isotopic variability during extreme tropical cyclones. *Nat. Commun.* https://doi.org/10.1038/s41467-019-12062-3 (2019).
46. Sánchez-Murillo, R., Durán-Quesada, A. M., Birkel, C., Esquivel-Hernández, G. & Boll, J. Tropical precipitation anomalies and d-excess evolution during El Niño 2014–16. *Hydrol. Process.* **31**, 956–967. https://doi.org/10.1002/hyp.11088 (2017).
47. Bong, H. & Yoshimura, K. *Enhancing the Representation of Atmospheric Water Isotopes with Higher-Resolution Global Modeling (IsoGSM4)*. https://doi.org/10.5281/zenodo.14681370 (2025).
48. Bardales, W. A., Campos, L., Gómez, R., Ordóñez, S. & Machuca, N. Variabilidad y Cambio Climatico en Guatemala. 147 (Instituto Nacional de Sismología, Vulcanología, Meteorología e Hidrología, 2019).
49. Poveda, G., Waylen, P. R. & Pulwarty, R. S. Annual and inter-annual variability of the present climate in northern South America and southern Mesoamerica. *Palaeogeogr. Palaeoclimatol. Palaeoecol.* **234**, 3–27. https://doi.org/10.1016/j.palaeo.2005.10.031 (2006).
50. Durán-Quesada, A. M., Sorí, R., Ordoñez, P. & Gimeno, L. Climate perspectives in the Intra-Americas Seas. *Atmosphere* https://doi.org/10.3390/atmos11090959 (2020).
51. Taylor, M. A. Influence of the tropical Atlantic versus the tropical Pacific on Caribbean rainfall. *J. Geophys. Res.* https://doi.org/10.1029/2001jc001097 (2002).
52. Taylor, M. A., Stephenson, T. S., Owino, A., Chen, A. A. & Campbell, J. D. Tropical gradient influences on Caribbean rainfall. *J. Geophys. Res. Atmos.* https://doi.org/10.1029/2010jd015580 (2011).
53. Taylor, M. A. & Alfaro, E. J. in *Encyclopedia of World Climatology Encyclopedia of Earth Sciences Series* Ch. Chapter 37, 183–189 (Springer Netherlands, 2005).
54. Giannini, A., Kushnir, Y. & Cane, M. Giannini A, Kushnir Y, Cane MA. Interannual variability of Caribbean rainfall, ENSO, and the Atlantic Ocean. Journal of Climate. *Journal of Climate J CLIMATE* **13**, 297–311, (2000).
55. Martinez, C., Goddard, L., Kushnir, Y. & Ting, M. Seasonal climatology and dynamical mechanisms of rainfall in the Caribbean. *Clim. Dyn.* **53**, 825–846. https://doi.org/10.1007/s00382-019-04616-4 (2019).
56. Magaña, V., Amador, J. A. & Medina, S. The midsummer drought over Mexico and Central America. *J. Clim.* **12**, 1577–1588 (1999).
57. Wang, C. Variability of the Caribbean low-level jet and its relations to climate. *Clim. Dyn.* **29**, 411–422. https://doi.org/10.1007/s00382-007-0243-z (2007).
58. Hidalgo, H. G., Durán-Quesada, A. M., Amador, J. A. & Alfaro, E. J. The Caribbean low-level jet, the inter-tropical convergence zone and precipitation patterns in the intra-Americas sea: A proposed dynamical mechanism. *Geogr. Ann. Ser. B* **97**, 41–59 (2015).
59. Small, R. J. O., De Szoeke, S. P. & Xie, S.-P. The central American midsummer drought: regional aspects and large-scale forcing. *J. Clim.* **20**, 4853–4873. https://doi.org/10.1175/jcli4261.1 (2007).
60. Wang, C., Enfield, D. B., Lee, S.-K. & Landsea, C. W. Influences of the Atlantic warm pool on Western Hemisphere summer rainfall and Atlantic hurricanes. *J. Clim.* **19**, 3011–3028. https://doi.org/10.1175/jcli3770.1 (2006).
61. Sáenz, F. & Durán-Quesada, A. M. A climatology of low level wind regimes over Central America using a weather type classification approach. *Front. Earth Sci.* https://doi.org/10.3389/feart.2015.00015 (2015).
62. Huffman, G. J. *et al.* NASA Global precipitation measurement (GPM) integrated multi-satellite retrievals for GPM (IMERG) version 07. *Algorithm Theoretical Basis Document (ATBD) Version* **47** (2023).
63. Breitenbach, S. F. et al. Strong influence of water vapor source dynamics on stable isotopes in precipitation observed in Southern Meghalaya, NE India. *Earth Planet. Sci. Lett.* **292**, 212–220 (2010).
64. Natali, S. et al. Assessing moisture origin as a potential driver of event-based precipitation isotope variability in a Western Mediterranean catchment (Apuan Alps, Italy). *Clim. Dyn.* **63**, 159. https://doi.org/10.1007/s00382-025-07650-7 (2025).
65. Tang, Y. et al. Using stable isotopes to understand seasonal and interannual dynamics in moisture sources and atmospheric circulation in precipitation. *Hydrol. Process.* **31**, 4682–4692. https://doi.org/10.1002/hyp.11388 (2017).
66. Lachniet, M. S., Patterson, W. P., Burns, S., Asmerom, Y. & Polyak, V. Caribbean and Pacific moisture sources on the Isthmus of Panama revealed from stalagmite and surface waterδ18O gradients. *Geophys. Res. Lett.* https://doi.org/10.1029/2006gl028469 (2007).
67. Muñoz-Villers, L. E., González-Ríos, S. & Montero-Martínez, G. Moisture sources and synoptic-scale controls on wet season event rainfall in Mexico city: Evidence from stable isotopes. *Hydrol. Process.* **40**, e70486. https://doi.org/10.1002/hyp.70486 (2026).
68. Durán-Quesada, A. M., Gimeno, L. & Amador, J. Role of moisture transport for Central American precipitation. *Earth System Dynamics* **8**, 147–161. https://doi.org/10.5194/esd-8-147-2017 (2017).
69. Magaña, V. & Caetano, E. Temporal evolution of summer convective activity over the Americas warm pools. *Geophys. Res. Lett.* https://doi.org/10.1029/2004GL021033 (2005).
70. Taylor, M. & Alfaro, E. Climate of Central America and the Caribbean. In *The Encyclopedia of World Climatology* 183–189 (2005).
71. Friedman, I., Harris, J. M., Smith, G. I. & Johnson, C. A. Stable isotope composition of waters in the Great Basin, United States 1. Air-mass trajectories. *J. Geophys. Res. Atmos.* **107**, ACL 14-11-ACL 14-14 (2002).
72. Joe Lambert, W. & Aharon, P. Oxygen and hydrogen isotopes of rainfall and dripwater at DeSoto Caverns (Alabama, USA): Key to understanding past variability of moisture transport from the Gulf of Mexico. *Geochimica et Cosmochimica Acta* **74**, 846–861, https://doi.org/10.1016/j.gca.2009.10.043 (2010).
73. Aemisegger, F. et al. Deuterium excess as a proxy for continental moisture recycling and plant transpiration. *Atmos. Chem. Phys.* **14**, 4029–4054. https://doi.org/10.5194/acp-14-4029-2014 (2014).
74. Gentine, P. et al. Land–atmosphere interactions in the tropics – a review. *Hydrol. Earth Syst. Sci.* **23**, 4171–4197. https://doi.org/10.5194/hess-23-4171-2019 (2019).
75. Smith, C., Baker, J. & Spracklen, D. Tropical deforestation causes large reductions in observed precipitation. *Nature*, 1–6 (2023).
76. Spracklen, D., Baker, J., Garcia-Carreras, L. & Marsham, J. The effects of tropical vegetation on rainfall. *Annu. Rev. Environ. Resour.* **43**, 193–218 (2018).
77. Kaseke, K. F. et al. Precipitation origins and key drivers of precipitation isotope (^{18}O, ^{2}H, and ^{17}O) compositions over Windhoek. *J. Geophys. Res. Atmos.* **123**, 7311–7330 (2018).
78. Sun, C. et al. 17O-excess in tropical cyclones reflects local rain re-evaporation more than moisture source conditions. *J. Geophys. Res. Atmos.* **129**, e2023JD039361 (2024).
79. Houze Jr, R. A. in *International geophysics* Vol. 104 141–163 (Elsevier, 2014).

80. Houze, R. A. Jr. Stratiform precipitation in regions of convection: A meteorological paradox?. *Bull. Am. Meteorol. Soc.* **78**, 2179–2196 (1997).
81. Houze, R. A. Jr. *Cloud Dynamics* Vol. 104 (Academic press, 2014).
82. Houze, R. A. Jr. Mesoscale convective systems. *Rev. Geophys.* https://doi.org/10.1029/2004RG000150 (2004).
83. Aggarwal, P., Schumacher, C., Funk, A. & Longstaffe, F. Water isotope ratios do reflect rain type proportions in the pantropics. (2024). https://doi.org/10.1126/sciadv.ado3258.
84. Landshuter, N., Aemisegger, F. & Mölg, T. Stable water isotope signals and their relation to stratiform and convective precipitation in the tropical andes. *J. Geophys. Res. Atmos.* https://doi.org/10.1029/2023jd040630 (2024).
85. Zuluaga, M. D. & Houze, R. A. Extreme convection of the near-equatorial Americas, Africa, and adjoining oceans as seen by TRMM. *Mon. Weather Rev.* **143**, 298–316. https://doi.org/10.1175/MWR-D-14-00109.1 (2015).
86. Waliser, D. E., Graham, N. E. & Gautier, C. Comparison of the highly reflective cloud and outgoing longwave radiation datasets for use in estimating tropical deep convection. *J. Clim.* **6**, 331–353. https://doi.org/10.1175/1520-0442(1993)006%3c0331:cothrc%3e2.0.co;2 (1993).
87. Vimeux, F., Tremoy, G., Risi, C. & Gallaire, R. A strong control of the South American SeeSaw on the intra-seasonal variability of the isotopic composition of precipitation in the Bolivian Andes. *Earth Planet. Sci. Lett.* **307**, 47–58. https://doi.org/10.1016/j.epsl.2011.04.031 (2011).
88. Evans, J. L. & Webster, C. C. A variable sea surface temperature threshold for tropical convection. *Aust. Meteorol. Oceanogr. J.* **64**, S1–S8 (2014).
89. Risi, C. et al. What controls the isotopic composition of the African monsoon precipitation? Insights from event-based precipitation collected during the 2006 AMMA field campaign. *Geophys. Res. Lett.* https://doi.org/10.1029/2008GL035920 (2008).
90. Horel, J. D., Hahmann, A. N. & Geisler, J. E. An investigation of the annual cycle of convective activity over the tropical Americas. *J. Clim.* **2**, 1388–1403 (1989).
91. Kurita, N. Water isotopic variability in response to mesoscale convective system over the tropical ocean. *J. Geophys. Res. Atmos.* https://doi.org/10.1002/jgrd.50754 (2013).
92. Lacour, J.-L., Risi, C., Worden, J., Clerbaux, C. & Coheur, P.-F. Importance of depth and intensity of convection on the isotopic composition of water vapor as seen from IASI and TES δD observations. *Earth Planet. Sci. Lett.* **481**, 387–394. https://doi.org/10.1016/j.epsl.2017.10.048 (2018).
93. Risi, C., Bony, S., Vimeux, F., Chong, M. & Descroix, L. Evolution of the stable water isotopic composition of the rain sampled along Sahelian squall lines. *Q. J. R. Meteorol. Soc.* **136**, 227–242 (2010).
94. Lekshmy, P. R., Midhun, M., Ramesh, R. & Jani, R. A. 18O depletion in monsoon rain relates to large scale organized convection rather than the amount of rainfall. *Sci. Rep.* **4**, 5661. https://doi.org/10.1038/srep05661 (2014).
95. Misra, V., Li, H. & Kozar, M. The precursors in the Intra-Americas Seas to seasonal climate variations over North America. *J. Geophys. Res. Oceans* **119**, 2938–2948. https://doi.org/10.1002/2014JC009911 (2014).
96. Bernal, J. P. et al. High-resolution Holocene South American monsoon history recorded by a speleothem from Botuverá Cave Brazil. *Earth Planet. Sci. Lett.* **450**, 186–196. https://doi.org/10.1016/j.epsl.2016.06.008 (2016).
97. Lucia, G. et al. Late glacial to early Holocene hydroclimate and environmental changes in northern Central America coupled to upstream regional monsoon convection. *Geology* https://doi.org/10.1130/g54539.1 (2026).
98. Huth, T. E. et al. A framework for triple oxygen isotopes in speleothem paleoclimatology. *Geochim. Cosmochim. Acta* **319**, 191–219. https://doi.org/10.1016/j.gca.2021.11.002 (2022).
99. Sha, L. et al. A novel application of triple oxygen isotope ratios of speleothems. *Geochim. Cosmochim. Acta* **270**, 360–378 (2020).
100. Schreck, C. J. III., Lee, H.-T. & Knapp, K. R. H. HIRS outgoing longwave radiation—Daily climate data record: Application toward identifying tropical subseasonal variability. *Remote Sensing* **10**, 1325 (2018).
101. Liebmann, B. & Smith, C. A. Description of a complete (interpolated) outgoing longwave radiation dataset. *Bull. Am. Meteorol. Soc.* **77**, 1275–1277 (1996).
102. Iguchi, T. & Meneghini, R. (ed Goddard Earth Sciences Data and Information Services Center (GES DISC)) (Greenbelt, MD, 2021).
103. Schumacher, C. & Funk, A. Assessing convective-stratiform precipitation regimes in the tropics and extratropics with the GPM satellite radar. *Geophys. Res. Lett.* https://doi.org/10.1029/2023gl102786 (2023).
104. Schumacher, C. & Houze, R. A. Stratiform rain in the tropics as seen by the TRMM precipitation radar. *J. Clim.* **16**, 1739–1756. https://doi.org/10.1175/1520-0442(2003)016%3c1739:SRITTA%3e2.0.CO;2 (2003).
105. Bong, H. et al. Process-based intercomparison of water isotope-enabled models and reanalysis nudging effects. *J. Geophys. Res. Atmos.* **129**, 38719. https://doi.org/10.1029/2023JD038719 (2024).
106. Yoshimura, K., Kanamitsu, M., Noone, D. & Oki, T. Historical isotope simulation using reanalysis atmospheric data. *J. Geophys. Res. Atmos.* https://doi.org/10.1029/2008JD010074 (2008).
107. Cross, M. in *SciPy*. 133–137.
108. Warner, M. S. C. Introduction to PySPLIT: A Python toolkit for NOAA ARL's HYSPLIT model. *Comput. Sci. Eng.* **20**, 47–62. https://doi.org/10.1109/mcse.2017.3301549 (2018).
109. Stein, A. F. et al. NOAA's HYSPLIT atmospheric transport and dispersion modeling system. *Bull. Am. Meteor. Soc.* **96**, 2059–2077. https://doi.org/10.1175/bams-d-14-00110.1 (2015).
110. Nieto, R. & Gimeno, L. A database of optimal integration times for Lagrangian studies of atmospheric moisture sources and sinks. *Scientific Data* **6**, 59. https://doi.org/10.1038/s41597-019-0068-8 (2019).
111. Gimeno, L. et al. The residence time of water vapour in the atmosphere. *Nat. Rev. Earth Environ.* **2**, 558–569. https://doi.org/10.1038/s43017-021-00181-9 (2021).
112. Läderach, A. & Sodemann, H. A revised picture of the atmospheric moisture residence time. *Geophys. Res. Lett.* **43**, 924–933 (2016).
113. González-Méndez, I. et al. Oxygen isotopes in tree rings track neotropical climate dynamics. *Geophys. Res. Lett.* https://doi.org/10.1029/2025gl120744 (2026).
114. Wallace, J. M. & Hobbs, P. V. *Atmospheric Science: An Introductory Survey* Vol. Vol. 92 (Elsevier, 2006).
115. Bershaw, J., Penny, S. M. & Garzione, C. N. Stable isotopes of modern water across the Himalaya and eastern Tibetan Plateau: Implications for estimates of paleoelevation and paleoclimate. *J. Geophys. Res. Atmos.* https://doi.org/10.1029/2011JD016132 (2012).
116. Krklec, K., Domínguez-Villar, D. & Lojen, S. The impact of moisture sources on the oxygen isotope composition of precipitation at a continental site in central Europe. *J. Hydrol.* **561**, 810–821. https://doi.org/10.1016/j.jhydrol.2018.04.045 (2018).
117. Sodemann, H., Schwierz, C. & Wernli, H. Interannual variability of Greenland winter precipitation sources: Lagrangian moisture diagnostic and North Atlantic Oscillation influence. *J. Geophys. Res. Atmos.* https://doi.org/10.1029/2007jd008503 (2008).
118. Natali, S. et al. Moisture sources and climatic effects controlling precipitation stable isotope composition in a western Mediterranean island (Pianosa, Italy). *Atmos. Res.* **294**, 106987 (2023).
119. Krklec, K. & Domínguez-Villar, D. Quantification of the impact of moisture source regions on the oxygen isotope composition of precipitation over Eagle Cave, central Spain. *Geochim. Cosmochim. Acta* **134**, 39–54. https://doi.org/10.1016/j.gca.2014.03.011 (2014).
120. Baldini, L. M., McDermott, F., Baldini, J. U. L., Fischer, M. J. & Möllhoff, M. An investigation of the controls on Irish precipitation δ18O values on monthly and event timescales. *Clim. Dyn.* **35**, 977–993. https://doi.org/10.1007/s00382-010-0774-6 (2010).

121. Durán-Quesada, A. M., Gimeno, L., Amador, J. A. & Nieto, R. Moisture sources for Central America: Identification of moisture sources using a Lagrangian analysis technique. *J. Geophys. Res.* https://doi.org/10.1029/2009jd012455 (2010).
122. Dawdy, D. & Matalas, N. Vol. 8 (McGraw-Hill, 1964).
123. Dunn, O. J. Multiple comparisons among means. *J. Am. Stat. Assoc.* **56**, 52–64 (1961).
124. Šidák, Z. Rectangular confidence regions for the means of multivariate normal distributions. *J. Am. Stat. Assoc.* **62**, 626–633 (1967).

Acknowledgements

Special thanks to V. Atudorei at the Center of Stable Isotopes of the University of New Mexico for providing laboratory facilities for isotope analysis. We thank G. Jiang and M. Nicholl for the constructive feedback in the early stages of the research. Thanks to H. Bong and K. Yoshimura for granting access to IsoGSM4 data.

Author contributions

M.L., A.W. and G.L. designed the research; O.V. conducted rainfall sampling; G.L. and M.L. performed isotope analysis; D. Z. and G. L. collected gridded data and conducted correlation analysis; M.C.X. contributed to data collection; G.L. wrote the manuscript; D.Z, A.W., O.V, M.C.X., and M.L. contributed to the discussion and final draft of the manuscript.

Funding

The study was funded by collaborative National Science Foundation (NSF) research grant AGS 1804263 to M.L. and A.W. G.L was supported by the NSF grant AGS 1804263 and University of Nevada Top-tier doctoral graduate research assistantship (TTDGRA). The Geological Society of America Graduate Student Research grant to G.L funded sampling costs.

Declarations

Competing interests

The authors declare no competing interests.

Additional information

Supplementary Information The online version contains supplementary material available at https://doi.org/10.1038/s41598-026-63020-1.

Correspondence and requests for materials should be addressed to G.L.

Reprints and permissions information is available at www.nature.com/reprints.

Publisher's note Springer Nature remains neutral with regard to jurisdictional claims in published maps and institutional affiliations.

Open Access This article is licensed under a Creative Commons Attribution-NonCommercial-NoDerivatives 4.0 International License, which permits any non-commercial use, sharing, distribution and reproduction in any medium or format, as long as you give appropriate credit to the original author(s) and the source, provide a link to the Creative Commons licence, and indicate if you modified the licensed material. You do not have permission under this licence to share adapted material derived from this article or parts of it. The images or other third party material in this article are included in the article's Creative Commons licence, unless indicated otherwise in a credit line to the material. If material is not included in the article's Creative Commons licence and your intended use is not permitted by statutory regulation or exceeds the permitted use, you will need to obtain permission directly from the copyright holder. To view a copy of this licence, visit http://creativecommons.org/licenses/by-nc-nd/4.0/.

© The Author(s) 2026